Layer 5 of cortex innervates the thalamic reticular nucleus in mice

Briana J. Carroll[a], Vandana Sampathkumar[a,b] (iD), Narayanan Kasthuri[a,b], and S. Murray Sherman[a,1] (iD)

Neurons in the thalamic reticular nucleus (TRN) are a primary source of inhibition to the dorsal thalamus and, as they are innervated in part by the cortex, are a means of corticothalamic regulation. Previously, cortical inputs to the TRN were thought to originate solely from layer 6 (L6), but we recently reported the presence of putative synaptic terminals from layer 5 (L5) neurons in multiple cortical areas in the TRN [J. A. Prasad, B. J. Carroll, S. M. Sherman, *J. Neurosci.* 40, 5785–5796 (2020)]. Here, we demonstrate with electron microscopy that L5 terminals from multiple cortical regions make bona fide synapses in the TRN. We further use light microscopy to localize these synapses relative to recently described TRN subdivisions and show that L5 terminals target the edges of the somatosensory TRN, where neurons reciprocally connect to higher-order thalamus, and that L5 terminals are scarce in the core of the TRN, where neurons reciprocally connect to first-order thalamus. In contrast, L6 terminals densely innervate both edge and core subregions and are smaller than those from L5. These data suggest that a sparse but potent input from L5 neurons of multiple cortical regions to the TRN may yield transreticular inhibition targeted to higher-order thalamus.

thalamic reticular nucleus | layer 5 | corticothalamic

The flow of information between the cortex and dorsal thalamus is regulated to a significant extent by the thalamic reticular nucleus (TRN) (1–3), a major source of inhibition to the dorsal thalamus. Recent experiments in the TRN have demonstrated that discrete subpopulations in the TRN, with discrete localizations in the somatosensory sector of the TRN to the edge and core subregions, reciprocally connect with different subregions of the dorsal thalamus (i.e., neurons in the core TRN reciprocally connect to the first-order nucleus in the dorsal thalamus, the ventral posterior medial nucleus (VPm), and neurons along the edges of the TRN reciprocally connect to the higher-order nucleus in the dorsal thalamus, the posterior medial nucleus (POm) (4–6). These differences likely have functional implications, as first-order thalamic nuclei transmit information from subcortical structures to the cortex, and higher-order nuclei transmit information between cortical areas, serving as relays in transthalamic corticocortical pathways (7–9).

A remaining gap in the understanding of this circuit is the nature of cortical input. Previously, cortical inputs to the TRN were thought to arise solely from neurons of layer (L) 6 of the cortex (10, 11). However, more recent data suggest that L5 neurons from multiple cortical regions make putative synaptic terminals in the TRN and, in the case of primary cortex (S1), these L5 terminals concentrate along the edge of the TRN (12). Whether such terminals represent true synapses remains unexplored and has important implications for how cortical signals affect processing in the dorsal thalamus. In the present study, we aimed to determine if the varicosities from L5 in the TRN across cortical areas are indeed presynaptic terminals and how their location relates to core and edge subregions of the somatosensory TRN.

Results

Electron Microscopy.

L5 varicosities in the TRN are bona fide synaptic terminals. We used Cre-dependent adeno-associated viruses (AAVs) encoding enhanced ascorbate peroxidase (APEX2) to provide staining of axons and terminals visible with the electron microscope (13). We used the Cre-Lox strategy to target these axons and terminals from L5 cells; that is, we transfected L5 cells in Rpb4-Cre mice with two kinds of Cre-dependent APEX2 viruses, one labeling mitochondria (APX-M) and the other, cytoplasm (APX-C). These were delivered to four cortical sites, S1, primary motor cortex (M1), primary visual cortex (V1), and prefrontal cortex (PFC), in two mice (Fig. 1A). Different combinations of

Significance

The thalamic reticular nucleus provides inhibition to the dorsal thalamus and thus influences the transmission of information from the dorsal thalamus to the cortex. Here, we show this area receives inputs from a cortical lamina that drives feedforward transthalamic pathways through higher-order nuclei. We demonstrate that these inputs are synaptic using electron microscopy and that they target higher-order projecting reticular cells, presenting a means of gating transthalamic pathways.
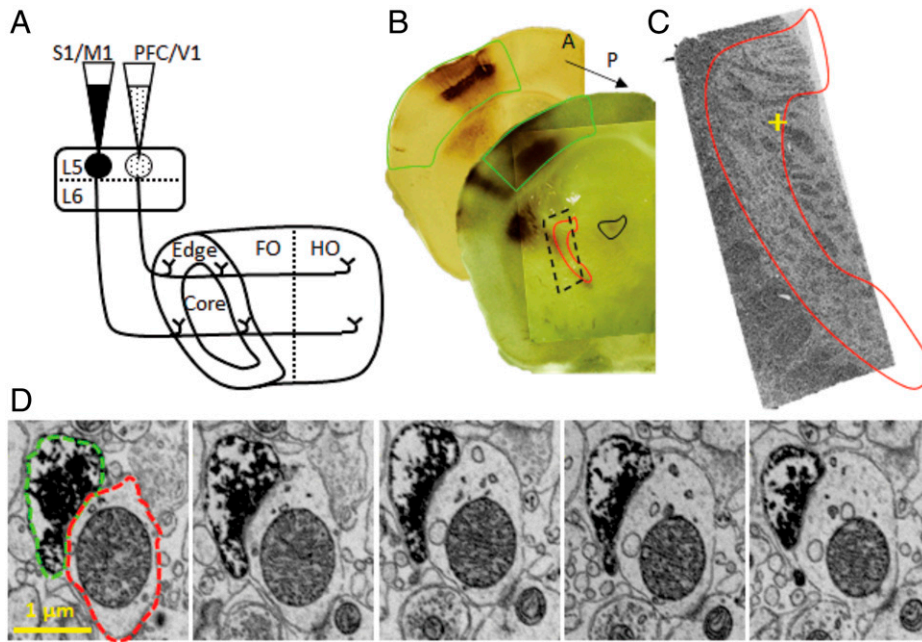
Fig. 1. Electron microscopy labeling of S1-L5 terminals in the TRN. (*A*) AAVs were injected in the cortex to orthogradely label L5 in S1, M1, V1, and PFC with APX. APX-C (solid) and APX-M (stippled) were injected in two separate cortical areas per mouse to label L5, resulting in two labels discriminable at the EM level (compare Figs. 1*D* and 2 *A–C*). (*B–D*) A representative case for the S1 injection site, where APX-C was injected. (*B*) Light micrograph of DAB immunoreactive coronal brain sections following injection in S1. Arrow indicates anterior-posterior relation between two sections. S1 is indicated in the sections by solid green outlines. The top section shows immunoreactive L5 cells at the injection site, and the bottom section includes labeling in the POm (solid black outline) and somatosensory TRN (solid red outline). The dashed box indicates the region dissected for EM imaging. (*C*) Low-resolution EM image of the dashed box in *B*. The yellow cross indicates the location of the synapse shown in *D*. (*D*) Serial sections cut at 40 nm through a representative APX-C–labeled S1 terminal in the TRN. The leftmost section is annotated to denote the APX-C–labeled S1 terminal (dashed green outline) and postsynaptic target (dashed red outline). FO, first-order thalamus; HO higher-order thalamus.

label and injection sites were used, yielding in the TRN both APX-M–labeled terminals in three animals ($n = 1$ in V1 and $n = 2$ in PFC) and APX-C–labeled terminals in 10 animals ($n = 3$ in S1, $n = 1$ in V1, $n = 3$ in PFC, and $n = 3$ in M1). Fig. 1 *B–D* shows results from a representative animal in which APX-C was injected into S1. Fig. 1*B* shows Di-Amino-Benzidine (DAB) immunoreactivity at the injection site (top section) and labeling seen in POm and somatosensory TRN (bottom section). The somatosensory subregion of the TRN was dissected and imaged at low resolution (Fig. 1*C*). For other injection sites, the appropriate level of TRN was dissected out (12). Terminals were identified across slices through the z-plane, and Fig. 1*D* shows a representative series of electron micrographs from the tissue in Fig. 1*C*, depicting a synapse made from a labeled L5 axon terminal (dashed green outline) originating in S1 and a dendrite (dashed red outline) in the TRN.

With our bulk labeling approach, we identified fields of terminals in each dissected TRN. An annotation of one such terminal field along the TRN's lateral border following injection in the M1 is shown in Fig. 2*A*. Fig. 2 *B–H* shows high-resolution images of individual terminals. In Fig. 2*C*, an APX-C–labeled terminal derived from L5 of S1 synapses onto the unlabeled TRN profile. The postsynaptic profile exhibits the usual postsynaptic density (red asterisks), and vesicles are present within the labeled terminal (green arrows), though somewhat obscured by the APX-C stain. These are more evident in terminals labeled with APX-M, as shown in Fig. 2 *E* and *G*, which shows analogous examples of L5 synapses onto TRN cells from V1 and PFC. This label darkly stains mitochondria (red crosses) compared to unlabeled mitochondria (blue crosses). Based on these structural features, we conclude that regardless of cortical subregion, L5 produces synaptic terminals in the TRN.

Light Microscopy.

L5 terminals preferentially target edge subregions of the TRN.
Having established that L5 varicosities seen with the light microscope are likely synapses, we used light microscopy to localize these varicosities TRN-wide. Because axons are sparse in the TRN (12), we performed bulk labeling of L5 neurons in the sensorimotor cortex using a Cre-dependent viral construct expressing enhanced yellow fluorescent protein (EYFP) in Rbp4-Cre mice ($n = 4$) (Fig. 3 *A, i*). We focused on the TRN's somatosensory sector (2), where core and edge subregions are most topographically distinct (4). We identified this sector as lying at the level of the POm. We observed that L5 axons traveling in the internal capsule pass medially through the TRN, bound for dorsal thalamic targets, including the POm. During their passage through the TRN, these L5 axons produced varicosities predominantly distributed along the medial and lateral boundaries of the TRN.

We localized the TRN with two counterstains: 1) labeling for the presence of GABAergic neurons (Fig. 4 *B, i*) and 2) labeling TRN cells in the edge regions projecting to the POm via a retrograde AAV injection in the POm (4–6). Fig. 3 *A* and *B* shows an example case; following injection in L5, terminals overlap with the thalamic injection site in the POm (Fig. 3 *A, ii*). In this example, the thalamic injection also spills medially to adjacent nuclei, including the parafascicular nucleus, which, like the POm, connects to the edge subpopulation (4). Following viral expression, we observed in the TRN labeled local anti–γ-aminobutyric acid (GABA)ergic cell bodies and labeled terminals likely derived from multiple afferents to the higher-order thalamus, including retrogradely labeled reticular cells, retrogradely labeled cortical cells, and higher-order relay cells, which were labeled at the injection site. At the level of the somatosensory TRN, this dense label flanked a largely unlabeled core (Fig. 3*B*), consistent with previous studies using the label from higher-order nuclei to
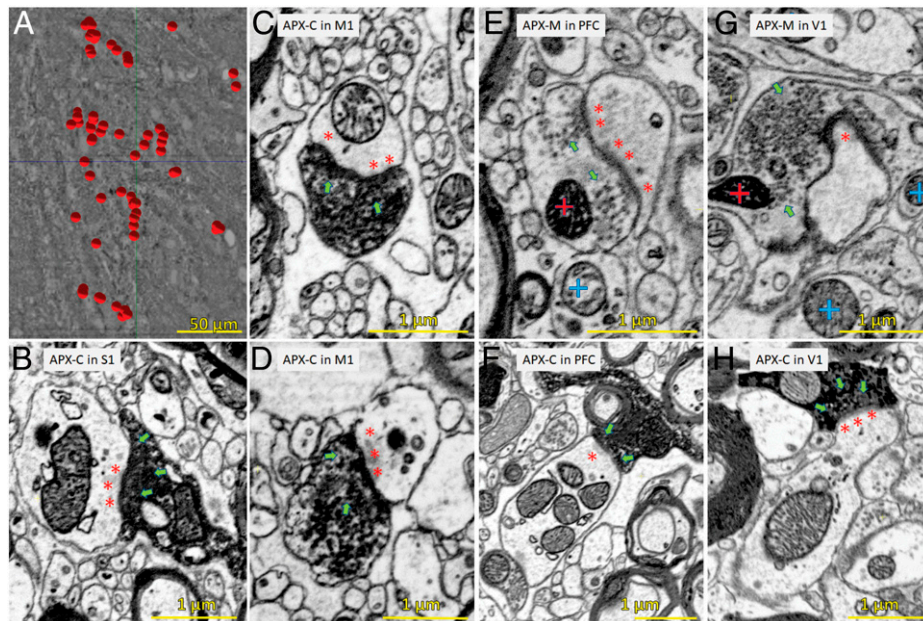
Fig. 2. L5 produces terminals in the TRN regardless of cortical area. (A) Field of annotated L5 terminals (red circles) in an edge region of the TRN derived from M1. (B–H) Representative terminals from different cortical injections. Green arrows denote presynaptic vesicles; red asterisks denote postsynaptic densities. Red crosses denote mitochondria labeled by APX-M, and for comparison, blue crosses denote unlabeled mitochondria in nearby structures. (B) APX-C–labeled L5 S1 terminal. (C and D) APX-C–labeled L5 M1 terminals. (E) APX-M–labeled L5 PFC terminal. (F) APX-C–labeled L5 PFC terminal. (G) APX-M–labeled L5 V1 terminal. (H) APX-C 431–labeled L5 V1 terminal.

label the edge (5, 6). Using this connectivity-based approach, we defined the TRN edge based on its connectivity with higher-order thalamus and the flanked core on its lack thereof.

We then characterized the distribution of L5 varicosities, which comingled with the TRN edge labeled from the thalamus (Fig. 3*B*). We sought to quantify this as follows: In a representative section from each of four animals, we imaged segments of the somatosensory TRN in which the edge subregions labeled from
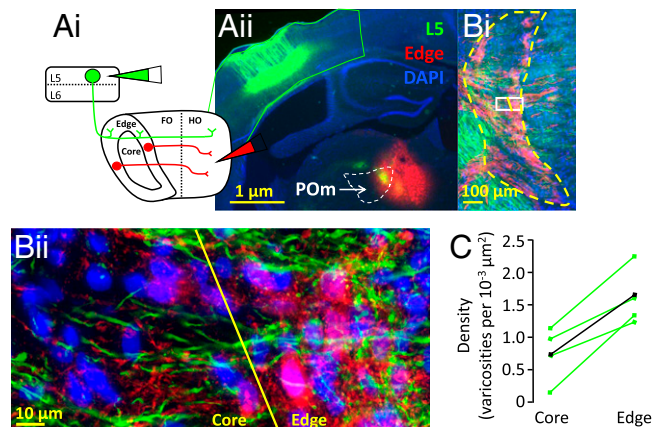

Fig. 3. L5 preferentially targets the TRN edge. (A) AAVs were injected in the cortex and thalamus to orthogradely label L5 cells in the cortex and retrogradely label TRN cells from HO thalamus. This is schematized in A, i, and a section containing representative injection sites is shown in A, ii. (A, ii) EYFP label in L5 at the injection site in S1 (green outline) and mCherry label at the injection site in higher-order thalamus. L5 axons in dorsal thalamus overlap with thalamic injection in the POm, resulting in yellow label. (B) Labeled L5 projections overlap with the retrolabeled population in the somatosensory TRN. (B, i) Low-power image of representative section including the TRN. Dashed yellow lines indicate TRN boundaries. The white box indicates area enlarged in B, ii, and the slanted yellow line within the box indicates the approximate boundary between an edge and core subregions of the TRN. (B, ii) Region shown in white box in B, i. (C) The density of L5 terminals encompassed in the TRN core and edge subregions. This density was significantly greater in the core for each individual animal (green) and for the average across animals (black). See Table 1 for details. FO, first-order thalamus; HO higher-order thalamus.

the higher-order POm exhibited clear flanking of the unlabeled core subregion. Using these images, we annotated labeled varicosities derived from L5. These annotations were performed blind to TRN subdivisions, which were annotated separately, using the label from the POm to identify medial and lateral edges and the unlabeled core in between. We then quantified the density of varicosities in each subregion. L5 terminals in the edge occurred at a density of 0.0016 per square micrometer, more than twice as common as in the core, where density was 0.0007 terminals per square micrometer. We used the nonparametric χ^2 test to confirm that this density differed between core and edge more than expected by chance, which was highly significant in each animal and across all four animals (Fig. 3*C* and Table 1).

L5 and L6 terminals in the TRN differ in localization and morphology. In the dorsal thalamus, terminal fields produced by L5 versus L6 exhibit differences in localization and morphology (10, 11). We examined whether the same is true in the TRN. To visualize these two populations in the same tissue in Rbp4-Cre mice ($n = 3$), we injected a mixture of Cre-dependent viral construct expressing EYFP and a construct not dependent on Cre-expressing mCherry, which labeled cells across cortical layers, including a mixed population of corticofugal cells in both L5 and L6 (Fig. 4*A*). L6 has previously been described as projecting to both the TRN core and edge subregions (14), and we similarly observed a label derived from the mixed L5/L6 population in both subregions of the TRN, including densely in the core of the TRN as shown in Fig. 4*B*. This was not evident among L5-labeled axons. Instead, as noted above, L5 varicosities were primarily restricted to the edges.

Compared to the large, sparse varicosities produced by exclusive labeling of L5 (Fig. 4 *C, i, iii*), the label from L6 densely filled the neuropil(Fig. 4 *C, ii*). Where these populations comingled in the medial edge of a representative section for each animal, we circled terminals from L5 and the mixed L5/L6 population to quantify their size. The resulting population histograms are shown in Fig. 4*D*. These distributions are consistent with previous such measurements of putative driver (e.g., L5 terminals here) versus modulator (L6 terminals) profiles (15); that is, the L5 terminals

Table 1. Density of L5 varicosities in TRN

		Core	Edge	P value
Animal 1	Varicosities	88	149	1.4695E-07
	Area (μm^2)	78,682.331	66,600.327	
Animal 2	Varicosities	57	110	0.0010177
	Area (μm^2)	80,124.245	90,992.121	
Animal 3	Varicosities	3	41	1.1997E-05
	Area (μm^2)	19,879.95	31,068.028	
Animal 4	Varicosities	89	71	0.00136539
	Area (μm^2)	92,008.43	44,319.596	
All	Varicosities	237	371	2.9507E-13
	Area (μm^2)	270,694.955	232,980.072	

(green bars) include a broad range of sizes, as reported previously for driver profiles. Modulator terminals have been described as uniformly small, and so we interpret the L5/L6 mixture of terminals (red bars) on the basis of the L6 terminals as being mainly responsible for the large peak of smaller profiles, whereas the L5 terminals in this population provide the tail of larger profiles. We compared L5 and L5/L6 populations using a Mann-Whitney U test to show L5 terminals were significantly larger than the mixed population. This was highly significant in each animal and across all three animals (Fig. 4D and Table 2). Thus, L5 afferents and L6 afferents to the TRN are different in their localization and morphology.

Discussion

We used electron microscopy to establish that L5 terminals from multiple cortical regions (e.g., somatosensory, visual, motor, and prefrontal) make ultrastructural bona fide synapses.

This finding challenges previous older assertions that cortical inputs to the TRN emanate solely from L6 (10, 11, 16, 17) and a more recent one that the L5 pathway to the TRN is restricted to that from the PFC (18, 19). Having validated with electron microscopy that varicosities seen at the light level are indeed synaptic terminals, we used light-level fluorescence microscopy to characterize the distribution of these terminals in the somatosensory sector of the TRN, where neurons in the core and edge reciprocally connect with VPm and POm neurons, respectively (4, 6). We found that L5 terminals preferentially target the edge of the TRN, synapsing with putative higher-order projecting TRN cells. This is in contrast to corticothalamic terminals from L6, which densely target both edge and core subregions of the TRN (14). Finally, we observed that varicosities emanating from L5 are larger than those from L6. This suggests that the L5 terminals have a driver function, indicating a particularly potent postsynaptic effect, although this clearly needs to be tested experimentally.
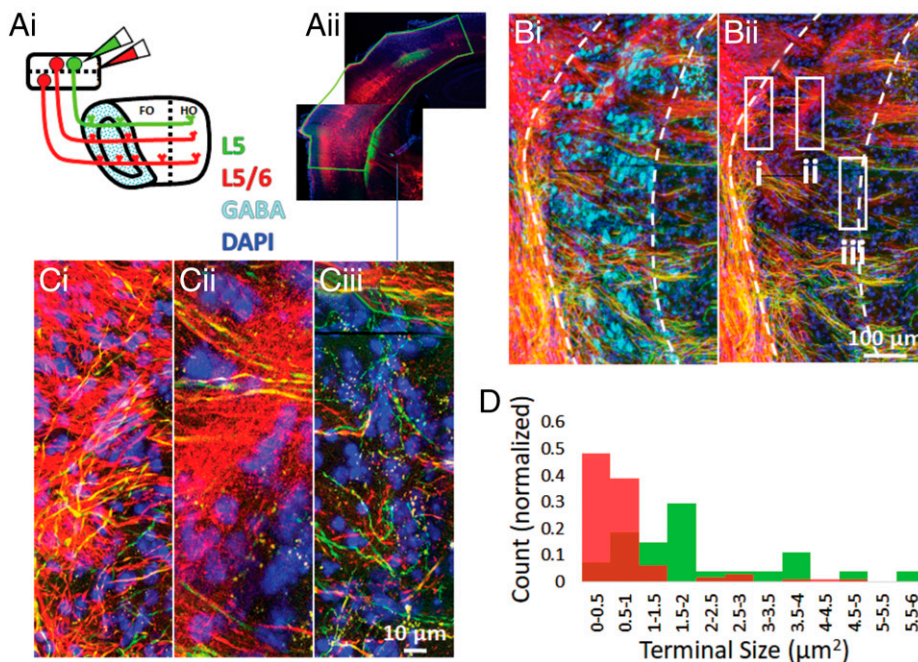

Fig. 4. Unlike L5, L6 terminals densely innervate the core. (A) AAVs were injected in the cortex. (A, i) Schematic illustrates the injections, which were a Cre-dependent vehicle to orthogradely label L5 (green) and a Cre-independent vehicle to label both L5 and L6 (red). Representative injection sites are shown in A, ii. (A, ii) Cells at the injection site in S1 (green outline) include a population labeled with EYFP (green label) restricted to L5, and a population labeled with mCherry (red label) that includes a mix of L5 and L6. (B) Resulting label in the TRN. Horizontal black lines are imaging artifacts. (B, i) Section including the TRN counterstained for GABA (cyan) to discriminate the TRN from surrounding regions. Dashed white lines indicate TRN borders. (B, ii) Same as B, i without GABA counterstain. Note the dense red label in the core of the TRN. Insets show the areas magnified in C. (C) C, i and C, iii show edge TRN subregions. Here, varicosities labeled with mCherry, EYFP, or both are common. In contrast, C, ii shows the TRN core subregion that is densely labeled with mCherry terminals, whereas EYFP label appears primarily as axons of passage. (D) Population histogram showing distribution of sizes of L5 terminals (green) and mixed L5/L6 terminals (red). L5 terminals were significantly larger than the mixed population including L6. (See Table 2 for values and text for details). FO, first-order thalamus; HO higher-order thalamus.

Table 2. Size of varicosities in TRN

		L5	L5/L6	U (Sum of ranks)	z-score	P value
Animal 1	Varicosities	10	28	35.5	−3.32	0.0009
	Mean size (μm^2)	2.90	0.85			
Animal 2	Varicosities	8	37	26	−3.61	0.0030
	Mean size (μm^2)	1.38	0.42			
Animal 3	Varicosities	9	41	81.5	−3.13	0.00174
	Mean size (μm^2)	1.60	0.91			
All	Varicosities	27	106	435	−5.83	<0.00001
	Mean size (μm^2)	1.98	0.73			

These findings add to a growing body of evidence that, like the dorsal thalamus, the TRN includes first-order (i.e., core) and higher-order (i.e., edge) subpopulations (Fig. 5). Beyond their reciprocal connectivity with nuclei of the same order in the dorsal thalamus (5, 6), we showed here that these subpopulations also resemble first- and higher-order dorsal thalamic nuclei in their pattern of cortical inputs: L5 corticothalamic axons preferentially target higher-order nuclei in the dorsal thalamus and, at least for the somatosensory sector, higher-order projecting subregions of the TRN. Whether this pattern extends to other sectors of the TRN, where the higher-order projecting subpopulation cannot easily be topographically discerned (4), remains to be examined. In contrast, L6 afferents target both first-order and higher-order nuclei of the dorsal thalamus (10, 11) and both first- and higher-order projecting subregions of the somatosensory TRN (14).

Our results provide a basis for reinterpreting previous studies that electrically or optically stimulated cortical inputs to the TRN (20, 21). Those authors described corticothalamic inputs as evoking larger excitatory post-synaptic potentials (EPSPs in TRN cells than in relay cells in the ventral posterior (VP) nucleus. Because it was then believed that only L6 axons innervated both structures, they attributed the differences to diverse synaptic properties

from the same branching axons onto the two targets, enabling these L6 axons to evoke larger responses in TRN cells. Our data suggest a different interpretation for their results: The cortical input to VP cells is indeed limited to L6, but that to TRN cells includes contributions from both L5 and L6, and the nature of these earlier studies was that both L5 and L6 corticothalamic cells would have been activated together. Since L5 corticothalamic inputs, where tested, evoke larger EPSPs than do those from L6 [reviewed in (3, 22)], we suggest that the explanation for the observed difference is not that L6 axons evoked larger EPSPs in the TRN than in the VP but rather the larger EPSPs seen in the TRN were a result of contributions from L5 input. Furthermore, the paired-pulse effects seen in the activation of VP cells showed less facilitation than those seen in TRN cells (20, 21), and considerable evidence indicates that while L6 inputs to the thalamus show facilitation, those from L5 show depression [reviewed in (3, 22)]; it follows that activating a pure L6 input (i.e., to the VP) would show more facilitation than activating a mixed L5 and L6 input (e.g., to the TRN) would.

As noted, it was previously thought that L5 inputs to the thalamus avoided the TRN, which corresponded to a similar picture for first-order thalamus; that is, driver input to first-order thalamus also avoided the TRN. The evidence for this
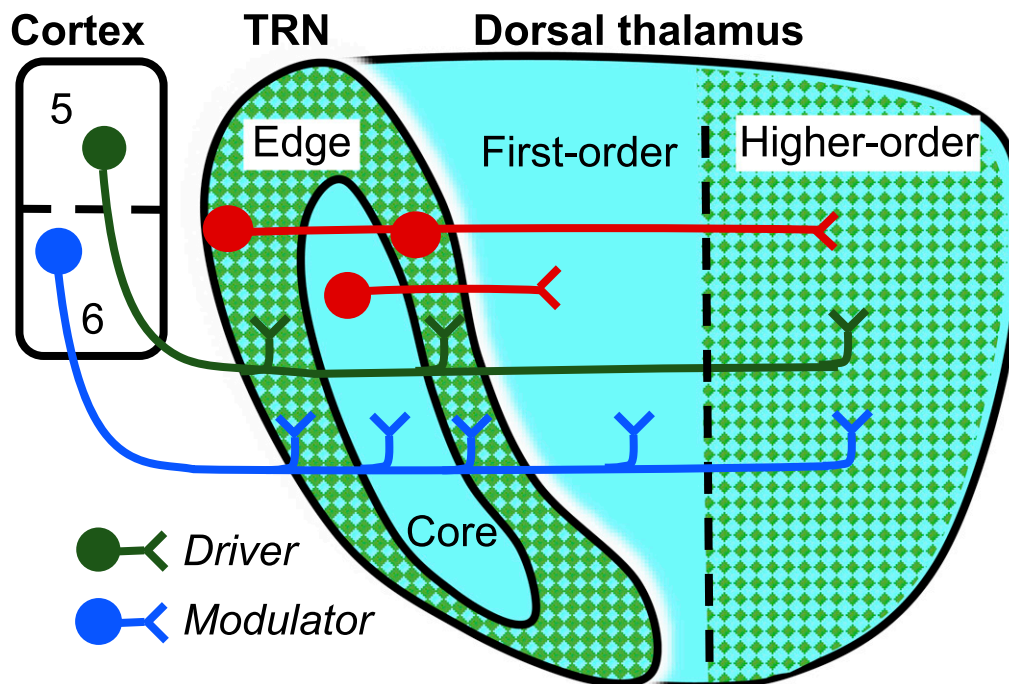

Fig. 5. Proposed cortico-TRN-thalamic circuits. Based on the observation that cortical afferents to the TRN resemble those to the dorsal thalamus, we propose edge and core are higher-order and first-order reticular subdivisions and that L6 inputs to both the TRN and dorsal thalamus are modulator, whereas those from L5 are driver.

almost exclusively stems from studies of the retinogeniculate pathway (3). However, a recent paper suggests that some retinal ganglion cells in the mouse do innervate the TRN (23). We suggest that the possibility needs to be reinvestigated more generally that there might be driver input to first-order thalamus that also innervates the TRN.

We thus conclude that the core and edge host cortico-reticulo-thalamic circuits with distinct inhibitory functions. L6 afferents innervate all subregions of the dorsal thalamus and TRN, and their inputs to relay cells appear to provide a modulatory role (3). In contrast, L5 afferents preferentially innervate the edge subregions of the TRN and higher-order nuclei; furthermore, L5 provides a driver input to relay cells in these higher-order nuclei and, as such, provide a transthalamic route for corticocortical communication (7–9). One reason to have such a message stream relayed through the thalamus is that these messages can be gated or modulated in ways unavailable to the message stream in direct corticocortical connections. The data we present here suggest a function for L5 outputs: These not only drive higher-order relay cells but also gate them through TRN processing, mostly involving TRN edge subregions of the TRN.

Methods

Experimental Design.

Stereotaxic surgery. All protocols were approved by The University of Chicago Institutional Animal Care and Use Committee. Transgenic mice were bred by crossing female C57BL6J mice with male Tg(Rbp4-Cre) KL100GSat/Mmcd mice (GENSAT RP24 -285K21), back-crossed with C57BL/6 mice, and maintained in a vivarium (conditions: 12-h light/dark cycle with food and water available ad libitum) (24). Littermates' tail biopsies were genotyped by Transnetyx to identify Rbp4-Cre–positive mice. This was ensured before performing stereotaxic, Cre-inducible DIO-AAV injections under aseptic conditions.

A total of 21 Rbp4-Cre mice (both males and females; 34 to 238 d old) were used in these experiments. Mice were deeply anesthetized, induced with 3% isoflurane and maintained throughout surgery with 2 to 2.5% isoflurane. All animals were monitored with toe pinches to ensure depth of anesthesia was maintained. They were head-fixed in a Kopf stereotaxic frame using bite and ear bars. The scalp was retracted, and a hand drill was used to expose the injection site. AAVs were injected using a 1-mL Hamilton syringe (catalog #14–824-20, Thermo Fisher Scientific) at coordinates determined using a stereotaxic atlas (25).

The syringe was slowly withdrawn, and the scalp incision was sutured closed. An antibiotic (Neosporin) and anesthetic (lidocaine hydrochloride) were topically applied to the sutures. The analgesic meloxicam was delivered subcutaneously (1 to 2 mg/kg dose) postoperatively and once every 24 h over 2 d.

Electron microscopy methods. Electron microscopy protocols followed those previously reported (13, 26). We employed the pea peroxidase APX 2.0 (27)] in a Cre-dependent fashion with one version targeting APX-C and the other to APX-M. AAV-CAG_DIO-APX2NES was a gift from Joshua Sanes, Harvard University, Cambridge, MA (Addgene plasmid no. 79907; http://www.addgene.org/79907; RRID: Addgene_79907). AAV-CAG-DIO-APEX2Mito was constructed in our laboratory as described previously (13). Both plasmids were packaged into rAAV9 at the Gene Therapy Center virus Vector Core facility at the University of North Carolina Chapel Hill: 500 nL was injected at 60 nL/min in S1 (from bregma, medial–lateral: ±3.1 mm, anterior–posterior: −0.9 mm; from cortical surface dorsal-ventral: −0.5 mm), M1 (from bregma, medial–lateral: ±2.5 mm, anterior–posterior: +1.54 mm; from cortical surface dorsal-ventral: −0.5 mm), V1 (from bregma, medial–lateral: ±2.5 mm, anterior–posterior: −3.5 mm; from cortical surface dorsal-ventral: −0.5 mm), or PFC (from bregma, medial–lateral: ±0.2 mm, anterior–posterior: +2.45 mm; from cortical surface dorsal-ventral: −0.8 mm).

At 19 to 54 d following injections, mice were deeply anesthetized with pentobarbital (60 mg/kg intraperitoneal; to be nonresponsive to toe pinch). The anesthetized mice were transcardially perfused with 10 mL 0.1 M cacodylate buffer followed by 20 mL of fixative solution composed of 2% paraformaldehyde (PFA) and 2.5% glutaraldehyde in 0.1 M cacodylate buffer. Each brain was removed, and 350-μm-thick coronal or Agmon-Connors sections (28) were cut using a vibratome. The sections were postfixed overnight at 4 °C in the same fixative described above. The sections were washed with cacodylate buffer and incubated in DAB for an hour followed by DAB with hydrogen peroxide for 20 to 30 min to visualize APX labeling (29). A visible brown precipitate was evaluated using a light microscope to make sure the appropriate injection sites S1, M1, V1, and prefrontal cortices and the corresponding target TRN sites were labeled. TRN was identified based on DAB staining and surrounding landmarks, and injection sites were localized based on staining intensity. Samples with appropriate staining were dissected out and subsequently prepared for visualization by electron microscopy. The tissues were stained with osmium, pyrogallol, reduced osmium followed by uranium, and lead. The tissues were then dehydrated in a series of ethanol and propylene oxide and embedded in epon (26). The 40- to 45-nm ultra-thin serial sections were cut using an ultramicrotome. The sections were collected on aluminum-coated Kapton tape using an automated tape-collecting ultramicrotome attached to 4-inch silicon wafers and carbon coated (30).

Ultrathin sections were imaged with a T1 segmented lower in-lens detector on Volumescope (Thermo Fisher Scientific) and Maps version 3.10. A series of 5 to 20, 1.5k × 1k, 5.4-nm high-resolution serial images were acquired at 1-μs dwell time. The TRN was identified using low-resolution images acquired at 1- to 2-μm resolution with reference to the DAB-stained light microscope image. Once the TRN subregion was identified, the sections were scanned to identify labeled terminals within the TRN subregion. The labeled terminals were visually identified by comparing the staining intensities of either the cytoplasm or mitochondria with unlabeled terminals. We looked for axonal swellings containing synaptic vesicles and postsynaptic densities on the target dendrites.

To assess terminal distribution in the TRN, about 1,500 40-nm sections were collected from M1-TRN; 372 ultrathin sections from M1-TRN and 305 ultrathin sections from S1-TRN were imaged with a T1 segmented lower in-lens detector on Volumescope (Thermo Fisher Scientific) and Maps version 3.10. M1-TRN was imaged at 20 nm x and y pixel resolution. M1-TRN low-resolution data were acquired as 5 × 2 tiles each 8k × 8k pixels, with 10% overlap to produce a final 36.8k × 15.2k-pixel image. The image was montaged and linearly aligned using a plugin, TrakEM2 on ImageJ, an open source image processing platform.

Linearly aligned stacks were further processed using aligntk (https://mmbios.pitt.edu/about-us/acknowledgements) on Cooley at Argonne National Laboratory. Aligned datasets were manually annotated for APX-M– and APX-C–labeled terminals using Knossos, a publicly available software, to identify the location of putative terminals in the low-resolution datasets. Each dataset was annotated by two manual annotators, and only those terminals agreed upon by both annotators were included.

Light microscopy methods. Light microscopy protocols followed those previously reported (12). For these experiments designed to selectively label cortical L5 neurons, 500 nL AAV-EF1a-DIO-hChR2(H134r)-EYFP-WPRE-pA (University of North Carolina at Chapel Hill Vector Core) were injected at 60 nL/min in each of four sites across the somatomotor cortex (S1 and M1 coordinates reported above and two additional sites: from bregma, medial–lateral: ±2.55 and 3.65 mm, anterior–posterior: 0.32 mm and −2.12 mm; from cortical surface dorsal-ventral: −0.5 mm). For light microscopy experiments also labeling L6, a 1:1 mixture of AAV-EF1a-DIO-hChR2(H134r)-EYFP-WPRE-pA to label L5 and AAV-hSyn-hChR2 (H134R)-EYFP (University of North Carolina at Chapel Hill Vector Core) to label across layers was injected at the four sites. To label the edge of the TRN, 90 nL pAAV-hysyn-mcherry (AddGene) was injected at 30 nL/min in the POm (from bregma, medial–lateral: ±1.25, anterior–posterior: −1.19 mm, dorsal-ventral: −3.5 mm).

At 14 to 19 d following injections, mice were deeply anesthetized with ketamine (100 mg/kg) and xylazine (3 mg/kg) and transcardially perfused with 1X phosphate-buffered saline (PBS) followed by 4% PFA. Brains were extracted and fixed overnight in 4% PFA or 30% sucrose in 4% PFA, then moved to 30% sucrose PBS for additional cryoprotection. Brains were flash-frozen using dry ice, mounted on a sliding microtome, and sectioned coronally at 50 μm. Every fourth section was rinsed in PBS, incubated with the nuclear marker DAPI, rinsed again in PBS, and mounted from dH$_2$0. Additional sections were stored at −20 °C in a cryoprotectant solution, and a subset of these were further processed for immunohistochemistry. These were rinsed in PBS, then incubated in a blocking solution composed of PBS with 0.3% Triton X-100 containing 4% bovine serum albumin for 1 h, incubated overnight in block solution

containing 1:250 rabbit GABA (#20094, IMMUNOSTAR) (31). After three 10-min PBS rinses, sections were incubated in blocking solution for 1 h, in blocking solution containing 1:100 Alexa Fluor 647 donkey anti-rabbit immunoglobulin G (H+L) (A31573 Invitrogen) for 2 h, and in PBS for three 10-min rinses. All sections were incubated with DAPI, rinsed again in PBS, mounted from dH$_2$0, and coverslipped with Vectashield antifade mounting medium (Vector Laboratories). Slides were stored at 4 °C to preserve the tissue's fluorescent signal.

Fluorescent slides were screened using a Leica Microsystems upright microscope fitted with fluorescence optics (100-W mercury lamp). Primarily, three filter cubes were used during screening: A4 (excitation 360 nm, emission 470 nm, dichroic 400 nm), L5 (excitation 480 nm, emission 527 nm, dichroic 505 nm), and TX2 (excitation 560 nm, emission 645 nm, dichroic 595 nm) to visualize signals for DAPI (blue channel), EYFP (green channel), and mCherry (red channel), respectively. Low-power (2.5 to 40) photomicrographs were captured using a Retiga 2000 monochrome CCD camera and QCapture imaging software (Teledyne QImaging).

Representative sections were chosen at the level of the POm for high-power imaging (63-100X) using an SP5 2-photon laser scanning confocal microscope (Leica Microsystems). The resulting images were annotated in ImageJ to localize anatomical regions of interest (ROIs): TRN edge retrolabeled from higher-order thalamus and unlabeled core. We also annotated labeled L5 terminals to assess the number present in each ROI. This number was divided by the ROI's area to calculate terminal density. We used the nonparametric χ^2 test to confirm that this value in edge was denser and in core was sparser than expected by pure chance.

Data, Materials, and Software Availability. Single electron microscopy images of labeled synapses and confocal stacks of multicolor fluorescence data have been deposited in https://github.com/carrolletal/carroll2021-L5-TRN-data- (32). Anonymized electron and light micrograph data have been deposited in https://github.com/carrolletal/carroll2021-L5-TRN-data- (32).

1. E. G. Jones, *The Thalamus* (Cambridge University Press, Cambridge, U.K., ed. 2, 2007).
2. D. Pinault, The thalamic reticular nucleus: Structure, function and concept. *Brain Res. Brain Res. Rev.* **46**, 1–31 (2004).
3. S. M. Sherman, R. W. Guillery, *Functional Connections of Cortical Areas: A New View from the Thalamus* (MIT Press, Cambridge, MA, 2013).
4. A. Clemente-Perez et al., Distinct thalamic reticular cell types differentially modulate normal and pathological cortical rhythms. *Cell Rep.* **19**, 2130–2142 (2017).
5. Y. Li et al., Distinct subnetworks of the thalamic reticular nucleus. *Nature* **583**, 819–824 (2020).
6. R. I. Martinez-Garcia et al., Two dynamically distinct circuits drive inhibition in the sensory thalamus. *Nature* **583**, 813–818 (2020).
7. C. Mo, S. M. Sherman, A sensorimotor pathway via higher-order thalamus. *J. Neurosci.* **39**, 692–704 (2019).
8. S. M. Sherman, Thalamus plays a central role in ongoing cortical functioning. *Nat. Neurosci.* **19**, 533–541 (2016).
9. B. B. Theyel, D. A. Llano, S. M. Sherman, The corticothalamocortical circuit drives higher-order cortex in the mouse. *Nat. Neurosci.* **13**, 84–88 (2010).
10. J. Bourassa, M. Deschênes, Corticothalamic projections from the primary visual cortex in rats: A single fiber study using biocytin as an anterograde tracer. *Neuroscience* **66**, 253–263 (1995).
11. J. Bourassa, D. Pinault, M. Deschênes, Corticothalamic projections from the cortical barrel field to the somatosensory thalamus in rats: A single-fibre study using biocytin as an anterograde tracer. *Eur. J. Neurosci.* **7**, 19–30 (1995).
12. J. A. Prasad, B. J. Carroll, S. M. Sherman, Layer 5 corticofugal projections from diverse cortical areas: Variations on a pattern of thalamic and extrathalamic targets. *J. Neurosci.* **40**, 5785–5796 (2020).
13. V. Sampathkumar, A. Miller-Hansen, S. M. Sherman, N. Kasthuri, Integration of signals from different cortical areas in higher order thalamic neurons. *Proc. Natl. Acad. Sci. U.S.A.* **118**, e2104137118 (2021).
14. C. M. Whilden, M. Chevée, S. Y. An, S. P. Brown, The synaptic inputs and thalamic projections of two classes of layer 6 corticothalamic neurons in primary somatosensory cortex of the mouse. *J. Comp. Neurol.* **529**, 3751–3771 (2021).
15. C. Mo, I. Petrof, A. N. Viaene, S. M. Sherman, Synaptic properties of the lemniscal and paralemniscal pathways to the mouse somatosensory thalamus. *Proc. Natl. Acad. Sci. U.S.A.* **114**, E6212–E6221 (2017).
16. S. Kakei, J. Na, Y. Shinoda, Thalamic terminal morphology and distribution of single corticothalamic axons originating from layers 5 and 6 of the cat motor cortex. *J. Comp. Neurol.* **437**, 170–185 (2001).
17. A. Hoerder-Suabedissen et al., Subset of cortical layer 6b neurons selectively innervates higher order thalamic nuclei in mice. *Cereb. Cortex* **28**, 1882–1897 (2018).
18. B. Zikopoulos, H. Barbas, Prefrontal projections to the thalamic reticular nucleus form a unique circuit for attentional mechanisms. *J. Neurosci.* **26**, 7348–7361 (2006).
19. N. A. Hadinger, E. Bősz, B. Tóth, G. Vantomme, A. Lüthi, L. Acsády, Region selective cortical control of the thalamic reticular nucleus. *bioRxiv* doi: 10.1101/2022.01.17.476335 (2021).
20. P. Golshani, X. B. Liu, E. G. Jones, Differences in quantal amplitude reflect GluR4- subunit number at corticothalamic synapses on two populations of thalamic neurons. *Proc. Natl. Acad. Sci. U.S.A.* **98**, 4172–4177 (2001).
21. S. J. Cruikshank, H. Urabe, A. V. Nurmikko, B. W. Connors, Pathway-specific feedforward circuits between thalamus and neocortex revealed by selective optical stimulation of axons. *Neuron* **65**, 230–245 (2010).
22. S. M. Sherman, W. M. Usrey, *Exploring Thalamocortical Interactions: Circuitry for Sensation, Action, and Cognition* (Oxford University Press, New York, 2021).
23. N. Parmhans et al., Identification of retinal ganglion cell types and brain nuclei expressing the transcription factor Brn3c/Pou4f3 using a Cre recombinase knock-in allele. *J. Comp. Neurol.* **529**, 1926–1953 (2021).
24. C. R. Gerfen, R. Paletzki, N. Heintz, GENSAT BAC cre-recombinase driver lines to study the functional organization of cerebral cortical and basal ganglia circuits. *Neuron* **80**, 1368–1383 (2013).
25. K. Paxinos, G. Franklin, *Paxinos and Franklin's The Mouse Brain in Stereotaxic Coordinates* (Elsevier Academic Press, 2013).
26. Y. Hua, P. Laserstein, M. Helmstaedter, Large-volume en-bloc staining for electron microscopy-based connectomics. *Nat. Commun.* **6**, 7923 (2015).
27. J. D. Martell, T. J. Deerinck, S. S. Lam, M. H. Ellisman, A. Y. Ting, Electron microscopy using the genetically encoded APEX2 tag in cultured mammalian cells. *Nat. Protoc.* **12**, 1792–1816 (2017).
28. A. Agmon, B. W. Connors, Thalamocortical responses of mouse somatosensory (barrel) cortex in vitro. *Neuroscience* **41**, 365–379 (1991).
29. S. S. Lam et al., Directed evolution of APEX2 for electron microscopy and proximity labeling. *Nat. Methods* **12**, 51–54 (2015).
30. N. Kasthuri et al., Saturated reconstruction of a volume of neocortex. *Cell* **162**, 648–661 (2015).
31. A. Eban-Rothschild et al., Arousal state-dependent alterations in VTA-GABAergic neuronal activity. *eNeuro* **7**, ENEURO.0356-19.2020 (2020).
32. B. J. Carroll, V. Sampathkumar, N. Kasthuri, S.M. Sherman, Layer 5 of cortex innervates the thalamic reticular nucleus in mice. GitHub. https://github.com/carrolletal/carroll2021-L5-TRN-data-. Deposited 30 August 2022.